Calculation of Magnetic Field Produced by OHTL under Normal and Abnormal Conditions

NAGAT M. K. ABDEL-GAWAD[1]
ADEL Z. EL DEIN[2]
MOHAMED MAGDY[1]
[1]Faculty of Engineering at Shoubra, Benha University, Cairo, Egypt
[2]Faculty of Energy Engineering, Aswan University, Aswan, Egypt

Abstract: - Ground level magnetic field from overhead transmission lines (OHTLs) is of increasingly important considerations in several research areas due to their harmful effect on human health and environment. This paper computes the ground level magnetic field, under normal and abnormal conditions of Egyptian 500-kV single circuit transmission line, in three dimension (3-D) coordinates by using 3-D integration technique. Abnormal conditions include symmetric fault, un-symmetric faults, direct stroke, and indirect stroke on the OHTL. Where, ATP software is used to simulate the OHTL under all faulty and lightning conditions. Varying time magnetic fields under normal and abnormal conditions, at certain points that located at mid-span, tower height and right-of-way (ROW), are also computed that to indicate the worst case.

Key-Words: - Magnetic field, Overhead transmission line, Normal and abnormal conditions, Right-of-way

1 Introduction

Considerable research and public attention triggered a wealth of research efforts focused on the evaluation of magnetic fields produced by overhead transmission lines (OHTLs) to insure the safety for human health which is recommended by world health organization (WHO) and American conference of governmental industrial hygienists (ACGIH) [1-6]. There are many researches deal with the calculation of the magnetic field under normal operating condition of the OHTL. An analytical calculation of the magnetic field produced by OHTLs, which is suitable for flat, vertical, or delta arrangement computed by complex vector method was produced in [7-8]. The estimation of the magnetic field density at points located under and far from the two parallel transmission lines with different design configurations was presented in [9-10]. In this paper, the time varying magnetic fields at specific points are calculated under normal and abnormal conditions of Egyptian 500 kV OHTL.

Under normal conditions, the effect of different percentages of load current on the calculated magnetic field is investigated. As well as, under abnormal conditions, the different type of faults and lightning, such as: single phase to ground fault, double phase to ground fault, phase to phase fault, three-phase to ground fault, direct stroke, and indirect stroke are investigated.

In this paper, the time varying magnetic fields are calculated at three different points: 1) under mid-span, 2) under tower height, and 3) at right-of-way, where the worst case under abnormal conditions is estimated. Also in this paper, the 3-D integration technique is used [11], where the effect of the conductor's sag is taken into consideration.

2 Magnetic Field Calculations

By using the 3-D Integration Technique, which explained in detail in [11] and is reviewed here, the magnetic field produced by a multiphase conductors (M), and their images, in support structures at any field point $P(x_o,y_o,z_o)$ shown in Fig. 1 can be obtained by using the Biot-Savart law as follow [11-12]:

The exact shape of a conductor suspended between two towers of equal height can be described by such parameters; as the distance between the points of suspension span L, the sag of the conductor S, the height of the lowest point above the ground h, and the height of the highest point above the ground hm, where $h_m - h = S$. Only two parameters are needed in order to define the shape of the catenary (S and L), while the third one (h or h_m), determines its location in relation to the ground surface.

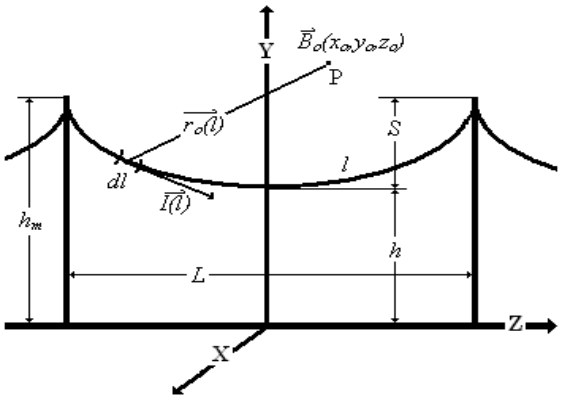

Fig. 1 Application of Biot-Savart law in three dimensions

Fig. 2 shows the basic catenary geometry for a single conductor line, this geometry is described by the following equation:

$$y = h + 2\alpha \sinh^2\left(\frac{z}{2\alpha}\right) \quad (1)$$

Where α is the solution of the transcendental equation:

$$h_m = h + 2\alpha \sinh^2\left(\frac{L}{4\alpha}\right)$$

The parameter α is also associated with the mechanical parameters of the line, $\alpha = T_h / w$ where T_h is the conductor tension at mid-span and w is the weight per-unit length of the line.

$$\vec{H}_o = \frac{1}{4\pi}\sum_{K=1}^{M}\sum_{n=-N}^{N}\int_{-L/2}^{L/2}\left[(H_x)_k \vec{a}_x + (H_y)_k \vec{a}_y + (H_z)_k \vec{a}_z\right]dz \quad (2)$$

Where:

$$(H_x)_k = I_k\left[(z - z_o + nL)\sinh(\frac{z}{\alpha_k}) - (y_k - y_o)\right]\Big/ d_k - I_k\left[(z - z_o + nL)\sinh(\frac{z}{\alpha_k}) - (y_k + y_o + 2\zeta)\right]\Big/ d`_k \quad (3)$$

$$(H_y)_k = \frac{I_k(x_k - x_o)}{d_k} - \frac{I_k(x_k - x_o)}{d`_k} \quad (4)$$

$$(H_z)_k = \frac{-I_k(x_k - x_o)\sinh(\frac{z}{\alpha_k})}{d_k} + \frac{I_k(x_k - x_o)\sinh(\frac{z}{\alpha_k})}{d`_k} \quad (5)$$

$$d_k = \left[(x_k - x_o)^2 + (y_k - y_o)^2 + (z - z_o + nL)^2\right]^{3/2} \quad (6)$$

$$d`_k = \left[(x_k - x_o)^2 + (y_k + y_o + 2\zeta)^2 + (z - z_o + nL)^2\right]^{3/2} \quad (7)$$

$\vec{a}_x$ Unit vector in X-direction,

$\vec{a}_y$ Unit vector in Y-direction,

$\vec{a}_z$ Unit vector in Z-direction.

The ζ is the complex depth of each conductor's image current which can be found as given in [12-13].

$$\zeta = \sqrt{2}\delta e^{-j\pi/4}\ ,\ \delta = 503\sqrt{\rho/f}$$

Where:

δ is the skin depth of the earth,

ρ is the resistivity of the earth, and

f is the frequency of the source current in Hz

The parameter (N) in equation (2) represents the number of spans to the right and to the left from the generic one where n=0 as shown in Fig. 2.

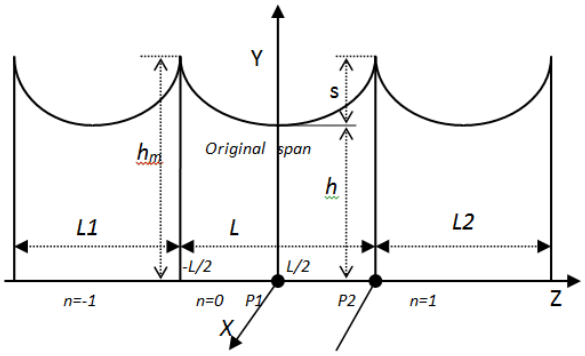

Fig. 2 Linear dimensions which determine parameters of the catenary

3 Results and Discussion

The data used in the calculation of the magnetic field density at points one meter above ground level (field points), under Egyptian 500-kV transmission-line single circuit are presented in appendix (A).

The phase-conductor currents are defined by a balanced direct-sequence three-phase set of 50 Hz sinusoidal currents, with 665-A rms, are shown in Fig. 3 and defined by the following equation:

$$I_p = 665\left[1; e^{-j2\pi/3}; e^{j2\pi/3}\right] \text{ A} \quad (8)$$

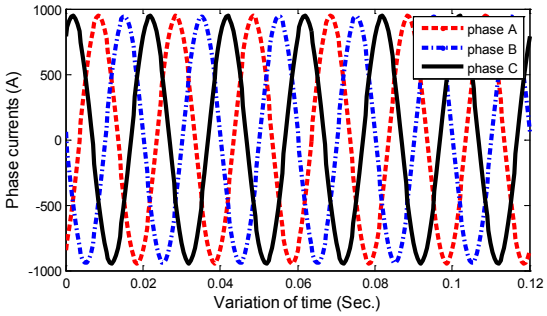

Fig. 3. Three phase 50 Hz sinusoidal currents under normal condition

1. Case(A): Magnetic field under normal condition

Figs. 4 and 5 shows the effect of the variation of the load capacity of the OHTL system (I_p) on the calculated magnetic field density under mid-span and under tower height and a distance away from the center phase, respectively. It is noticed that, the magnetic field density decreases with the decrease of the load capacity.

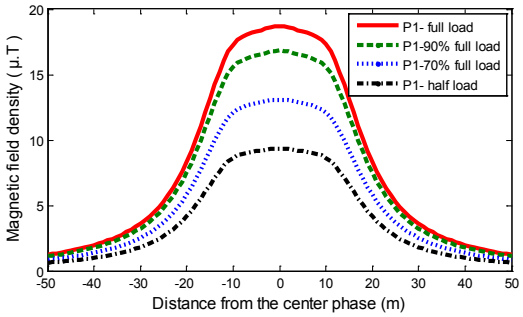

Fig. 4 Effect of load current on the magnetic field density at point (P1) under mid-span

According to [14], the value of magnetic field density at right-of-way is taken to be in range from 6.5 to 1.7 μ.T. In this paper, the ROW is assumed to be equal 25 m from the center phase [15]. From Figs. 4 and 5 it is noticed that the magnetic field density at ROW equals 5.3 μ.T under mid-span and 4.55 μ.T under tower height, respectively.

Fig. 6 shows the time variation of the calculated magnetic field density at mid-point under the center phase and at ROW, under the mid-span (point P1) and under the tower height (point P2). It is noticed that the maximum values of the calculated magnetic field densities occur under the mid-span.

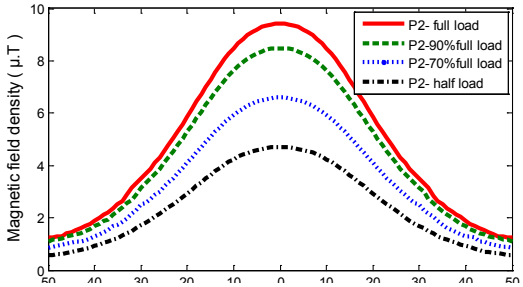

Fig. 5 Effect of load current on the magnetic field density at point (P2) under tower height

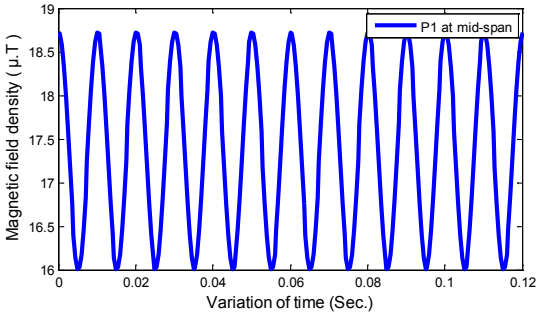

Fig. 6.a Varying time magnetic field density under mid-span (point P1) under normal condition

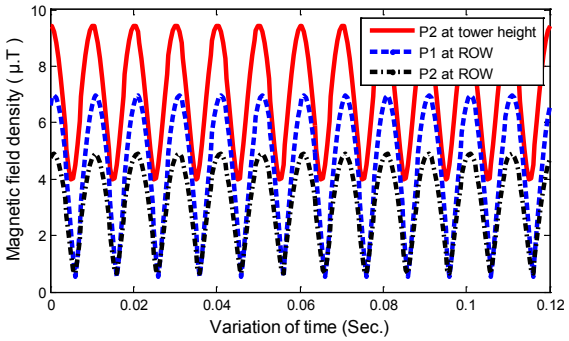

Fig. 6.b Varying time magnetic field density under tower height (point P2) and at ROW (point P1,P2) under normal condition

2. Case (B): Magnetic field under fault conditions

In case (B), the ATP software is used to simulate the OHTL under different fault conditions [16]. The fault is cleared after the time that is taken by the protection device. The time of the protection device is divided into high voltage SF6 circuit breaker breaking time that equals 40 msec. (2 cycle) [17], and the numerical distance relay time, which equals 12 msec [18]. So, the total fault clearing time equals 52 msec. Hence, the fault is assumed to be occurred at instant equals 0.03 second and is cleared after the

time that is taken by the protection device, at instant equals 0.082 second. The effects of various types of faults on the time varying magnetic field density are studied in this section.

2.a. Single phase to ground fault

Fig. 7 shows the three phase sinusoidal currents under single phase to ground fault on phase A, [0.03:0.082] sec, where, the maximum value of fault current tends to be 11 kA.

Fig. 8 shows the time varying magnetic field densities, during the single phase to ground fault, at mid-point (under the center phase) and at ROW under both mid-span (point P1) and tower height (point P2), respectively. It is seen that the maximum value of magnetic field density, during the fault period [0.03:0.082] sec., under mid-span (point P1), equals 170 μ.T.

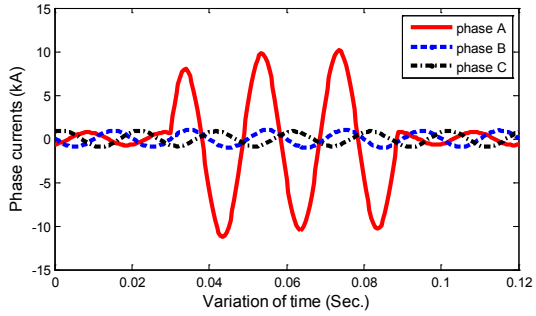

Fig. 7 Three phase sinusoidal currents under single phase to ground fault

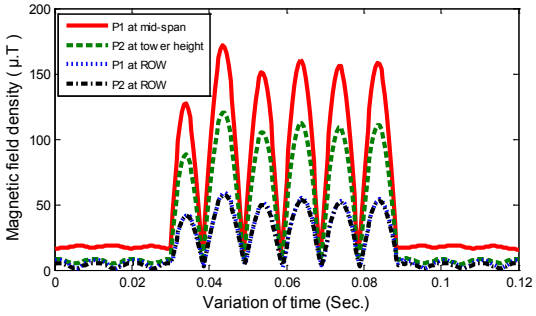

Fig. 8 Time varying magnetic field density at mid-point and at ROW under mid-span and under tower height (point P1, P2) under single phase to ground fault

2.b. Double phase to ground fault

Fig. 9 shows the three phase sinusoidal currents under double phase (A and B) to ground fault, [0.03:0.082] sec, where, the maximum value of fault current tends to be 20 kA.

Fig. 10 shows the time varying magnetic field densities, during the double phase to ground fault, at mid-point (under the center phase) and at ROW, under both mid-span (point P1) and tower height (point P2), respectively. It is seen that the maximum value of magnetic field density, during the fault period [0.03:0.082] sec, under mid-span (point P1), equals 430 μ.T.

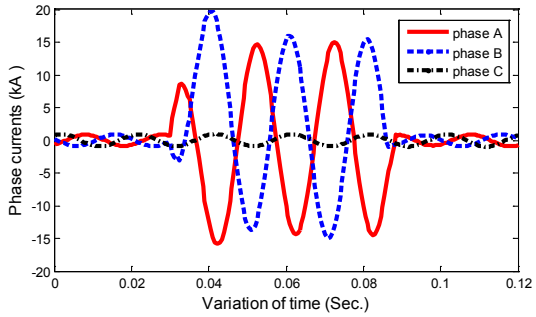

Fig. 9 Three phase sinusoidal currents under double phase to ground fault

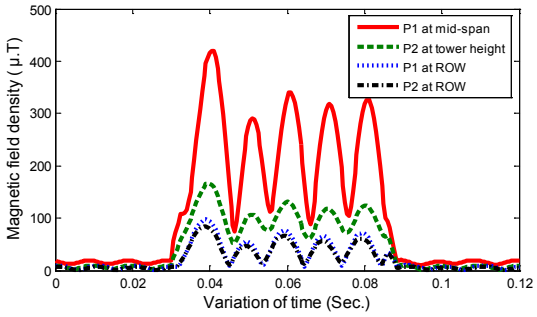

Fig. 10 Time varying magnetic field density at mid-point and at ROW under mid-span and under tower height (point P1,P2) under double phase to ground fault

2.c. Phase to phase fault

Fig. 11 shows the three phase sinusoidal currents under phase to phase (A and B) fault, for a period [0.03:0.082] sec, where, the maximum value of fault current tends to be 18 kA.

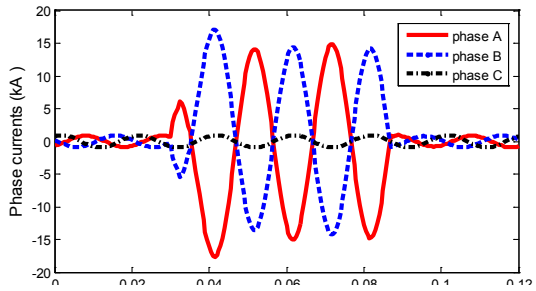

Fig. 11 Three phase sinusoidal currents under phase to phase fault

Fig. 12 shows the time varying magnetic field densities, during phase to phase fault, at mid-point (under the center phase) and at ROW, under both mid-span (point P1) and tower height (point P2), respectively. It is seen that the maximum value of magnetic field density, during the fault period [0.03:0.082] sec, under mid-span (point P1), equals 360 µ.T.

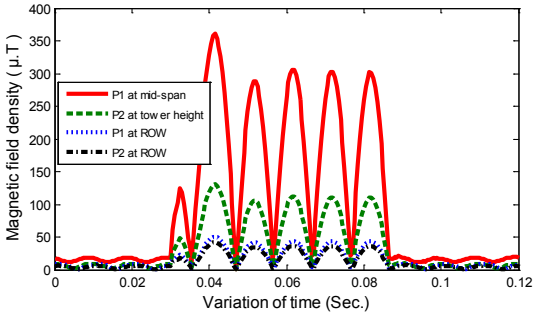

Fig. 12 Time varying magnetic field density at mid-point and at ROW under mid-span and under tower height (point P1,P2) under phase to phase fault

2.d. Three phase to ground fault

Fig. 13 shows the three phase sinusoidal currents, under three phase to ground fault, for a period [0.03:0.082] sec, where, the maximum value of fault current tends to be 21 kA.

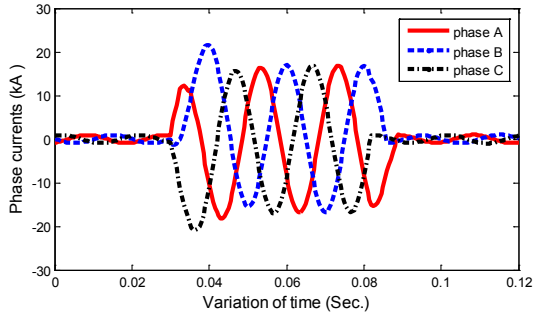

Fig. 13 Three phase sinusoidal currents under three phase to ground fault

Fig. 14 shows the time varying magnetic field densities, during the three phase to ground fault, at mid-point (under the center phase) and at ROW, under both mid-span (point P1) and tower height (point P2), respectively. It is seen that the maximum value of magnetic field density, during the fault period [0.03:0.082] sec, under mid-span (point P1), equals 400 µ.T.

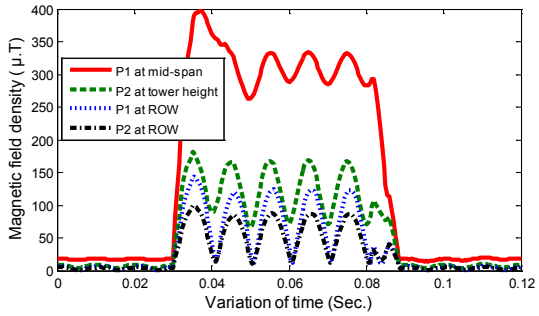

Fig. 14 Time varying magnetic field density at mid-point and at ROW under mid-span and under tower height (point P1, P2) under three phase to ground fault

From case (B), the worst effect of fault on the time varying magnetic field density is the double phase to ground fault, where the maximum value of the magnetic field density, during the fault period [0.03:0.082] sec under mid-span (point P1) equals 430 µ.T. Followed by three phase to ground fault, which have a maximum value of the magnetic field density equals 400 µ.T. Then phase to phase fault, which have a maximum value of the magnetic field density equals 360 µ.T. Finally, single phase to ground fault, which have a maximum value of the magnetic field density equals 170 µ.T.

3. Case (C):Magnetic field under lightning condition

In case (C), also ATP software is used to simulate the OHTL under lightning conditions. The lightning impulse is assumed to have the following parameters: peak value of 100 kA, channel resistance equals 1 MΩ, front time equals 4 µsec and tail time equals 50 µsec [19]. The effects of various type of lightning (direct and indirect) on the time varying magnetic field densities are studied in this section.

3.a. Direct stroke on phase (B)

Fig. 15 shows the three phase sinusoidal currents and ground wire currents under direct stroke on phase (B), where the currents in the two ground wires are equal, due to their relative position with respect to phase (B). It is noticed that the maximum value of the stroke current tends to be 50 kA within the first 4 µsec

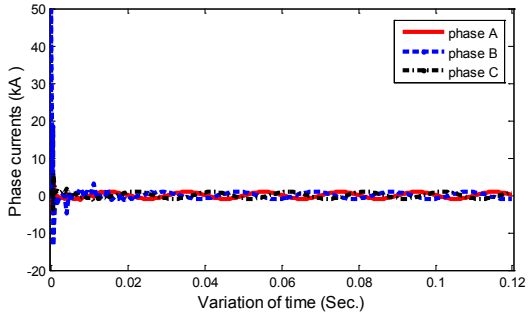

Fig. 15.a Three phase currents under direct stroke on phase B

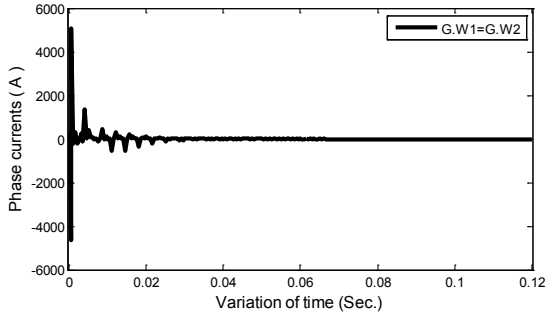

Fig. 15.b Ground wire currents under direct stroke on phase B.

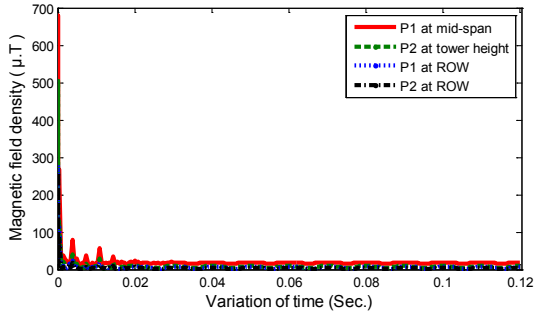

Fig. 16 Time varying magnetic field density at mid-point and at ROW under mid-span and under tower height (point P1, P2) under direct stroke on phase B

Fig. 16 shows the time varying magnetic field densities, during the direct lightning stroke on phase B, at mid-point (under the center phase) and at ROW, under both mid-span (point P1) and tower height (point P2), respectively. It is seen that the maximum value of magnetic field density, under mid-span (point P1), equals 680 µ.T.

3.b. Indirect stroke on ground wire (1)

Fig. 17 shows the three phase sinusoidal currents and ground wire currents under indirect stroke on ground wire (1). It is noticed that the maximum value of stroke current tends to be 50 kA within the first 4 µsec.

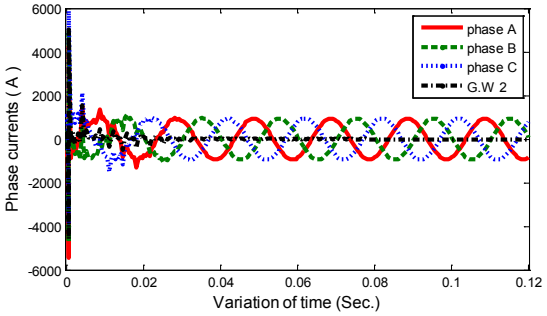

Fig. 17.a Three phase and G.W2 currents under indirect stroke on G.W1

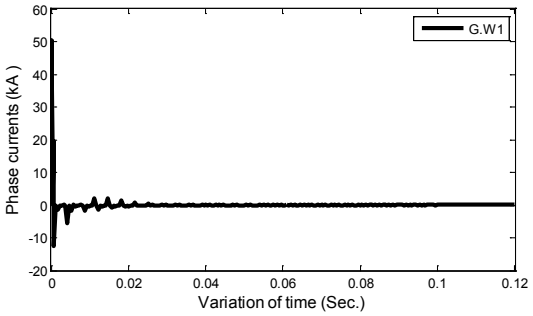

Fig. 17.b Ground wire (1) current under indirect stroke on G.W1

Fig. 18 shows the time varying magnetic field densities, during the indirect lightning stroke on ground wire (1), at mid-point (under the center phase) and at ROW, under both mid-span (point P1) and tower height (point P2), respectively. It is seen that the maximum value of magnetic field density, under mid-span (point P1), equals 460 µ.T.

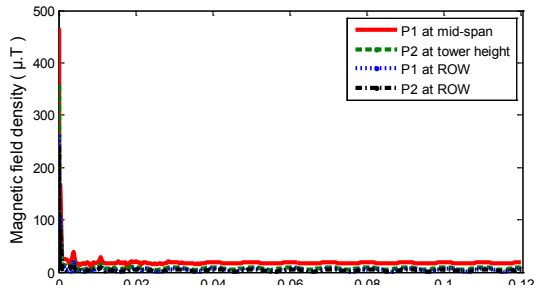

Fig. 18 Time varying magnetic field density at mid-point and at ROW under mid-span and under tower height (point P1, P2) under indirect stroke on ground wire (1)

4 Conclusion

In this paper the time varying magnetic field densities are calculated and analyzed under three different cases of the OHTL namely: normal operating, fault, and lightning conditions.

At normal operating condition, the magnetic field density varies with the distance from the center phase for different percentage of load current. Also, the decrease in the load capacity decreases the magnetic field density. Due to the sag effect, the ground level magnetic field density has its maximum value under the mid-span, where, the clearance between the conductors and the ground level has its minimum value. But under tower height, the ground level magnetic field density has its minimum value due to the maximum clearance between the conductors and the ground level.

Under different faulty conditions, it is observed that the highest values of the time varying magnetic field densities at certain points (mid-span, tower height, and ROW) are obtained firstly under double phase to ground fault, then under three phase to ground fault, then under phase to phase fault, and finally under single phase to ground fault, which has the lowest value.

Under lightning conditions, it is clear that the calculated values of the time varying magnetic field densities at certain points for direct lightning stroke are more dangerous than those of indirect lightning stroke and of different faulty conditions, even if, it is rarely happen.

References:

[1] H. Karawia, K. Youssef and A. A. Hossam-Eldin, "Measurements and Evaluation of Adverse Health Effects of Electromagnetic Fields from Low Voltage Equipments" MEPCON 2008, Aswan, Egypt, PP. 436- 440, March 12-15, 2008.

[2] Ahmed A. Hossam-Eldin, "Effect of Electromagnetics Fields from Power Lines on Living Organisms" IEEE 7th International Conference on Solid Dielectrics, Eindhoven, the Netherlands, pp. 438-441, June 25-29, 2001.

[3] T. Dan Bracken, "North steens Transmission Line Project-Appendix C: Electrical Effects" New York-America, PP. 10-14, February 2010.

[4] IEEE Standard Procedures for Measurement of Power Frequency Electric and Magnetic Fields from AC Power Lines. ANSI/IEEE Std., New York, NY, PP. 644-1994.

[5] S. M. Abd-Elazim, and E. S. Ali, “Synergy of Particle Swarm Optimization and Bacterial Foraging for TCSC Damping Controller Design”, Int. J. of WSEAS Transactions on Power Systems, Vol. 8, No. 2, April 2013, pp. 74-84.

[6] S. M. Abd-Elazim, and E. S. Ali, “Bacteria Foraging: A New Technique for Optimal Design of FACTS Controller to Enhance Power System Stability”, International Journal WSEAS Transactions on Systems, Vol. 12, No. 1, January 2013, pp. 42-52.

[7] G. Filippopoulos and D. Tsanakas, "Analytical calculation of the magnetic field produced by electric power lines " IEEE Transactions on Power Delivery, vol. 20, no. 2, pt. 2, pp. 1474–1482, April 2005.

[8] F. Moro and R. Turri, "Fast analytical computation of power-line magnetic fields by complex vector method " IEEE Transactions on Power Delivery, vol.23, no. 2, pp. 1042–1048, October 2008.

[9] A. A. Dahab, F. K. Amoura, and W. S. Abu-Elhaija, "Comparison of magnetic-field distribution of non-compact and compact parallel transmission-line configurations "

IEEE Transactions on Power Delivery, vol. 20, no. 3, pp. 2114–2118, July 2005.

[10] W. T. Kaune and L. E. Zaffanella, "Analysis of magnetic fields produced far from electric power lines " IEEE Transactions on Power Delivery, vol. 7, no. 4, pp. 2082–2091, October 1992.

[11] Adel Z. El Dein, "Magnetic Field Calculation under EHV Transmission Lines for More Realistic Cases " IEEE Transactions on Power Delivery, Vol. 24, No. 4, pp. 2214-2222, October 2009.

[12] R. D. Begamudre, "Extra High Voltage AC. Transmission Engineering" Wiley Eastern Limited, third Edition, Book, Chapter 7, pp.172-205, 2006.

[13] A. V. Mamishev, R. D. Nevels, and B. D. Russell, "Effects of Conductor Sag on Spatial Distribution of Power Line Magnetic Field" IEEE Transactions on Power Delivery, Vol. 11, No. 3, pp. 1571-1576, July 1996.

[14] T. Dan Bracken, "Big Eddy – Knight 500-KV Transmission Project-Appendix E: Electric Fields, Magnetic Fields, Noise, and Radio Interference " Ch.4, pp. 8-12, march 2010.

[15] F. Moustafa, E. moustafa, H. Ahmed, and M. Ismail "Consideration of Magnetic Field Levels in Designing Transmission Lines and Substations for Residentially Crowded Areas in Egypt", Cigre Session 2004.

[16] ATP Draw – User manual, available online: www.atpdraw.net/getipdf. php?myfile=ATPDMan5.6p.pdf

[17] S. Catalogue, " High-Voltage Circuit-Breakers 3AP1/2 with rated from 72.5 kV up to 550 kV ", Technical Data, pp.1-11.

[18] ABB Catalogue, " Numerical Distance Relay REL 301/302 Version 1.4 "Section 1: Technical Specifications, pp.7-9, April 1996.

[19] J. Rohan Lucas, "High Voltage Engineering", Second Edition, Book, Chapter 3, pp. 34 – 43, Sri Lanka, October 2001.

APPENDIX A

Fig. A1 and Table A1 give the configuration and data of the El-Kuorimate-Cairo power line, which are used in the calculation of the magnetic field.

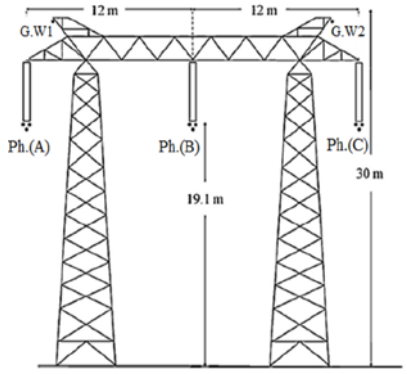

Fig. A1 Power line tower dimensions of 500 kV

Table A1
El-Kuorimate-Cairo power line.

Item	Value
MVA	575
Line voltage (r.m.s) in kV	500
Length in km	124
Positive & negative sequence impedance per phase in ohm	3.307+ j14.053
Zero sequence impedance per phase in ohm	10.75+j45.67
No. of circuits per tower	1
No. of sub-conductors per phase	3
No. of ground wires	2
Diameter of sub-conductor in mm	30.6
Spacing between sub-conductor in phase in cm	47
Span in meter	400
Spacing between center phase and ground wire in meter	10
Vertical height of conductor at mid-span in meter	9
Vertical height of ground wire at mid-span in meter	21
Diameter of ground wire in mm	11.02
DC resistance of conductor in ohm per km	0.0133
DC resistance of ground wire in ohm per km	0.35